Supplemental Information:

Direct recordings of grid-like neuronal activity in human spatial navigation

Joshua Jacobs[1], Christoph T. Weidemann[2], Jonathan F. Miller[1], Alec Solway[3], John Burke[4], Xue-Xin Wei[4], Nanthia Suthana[5], Michael Sperling[6], Ashwini D. Sharan[7], Itzhak Fried[5,8*], & Michael J. Kahana[4*]

[1] School of Biomedical Engineering, Science & Health Systems, Drexel University, Philadelphia, PA 19104
[2] Department of Psychology, Swansea University, Singleton Park, Swansea, SA2 8PP, Wales, UK
[3] Princeton Neuroscience Institute, Princeton University, NJ 08544
[4] Department of Psychology, University of Pennsylvania, Philadelphia, PA 19104
[5] Department of Neurosurgery, David Geffen School of Medicine and Semel Institute for Neuroscience and Human Behavior, University of California, Los Angeles, CA 90095
[6]Department of Neurology, Thomas Jefferson University, Philadelphia, PA 19107
[7]Department of Neurosurgery, Thomas Jefferson University, Philadelphia, PA 19107
[8]Functional Neurosurgery Unit, Tel-Aviv Medical Center and Sackler Faculty of Medicine, Tel-Aviv University, Tel-Aviv 69978, Israel
$*$ denotes equal contributions

Address correspondence to:
- Dr. Joshua Jacobs (Drexel University, joshua.jacobs@drexel.edu)
- Dr. Michael J. Kahana (University of Pennsylvania, kahana@psych.upenn.edu)
- Dr. Itzhak Fried (University of California, ifried@mednet.ucla.edu)

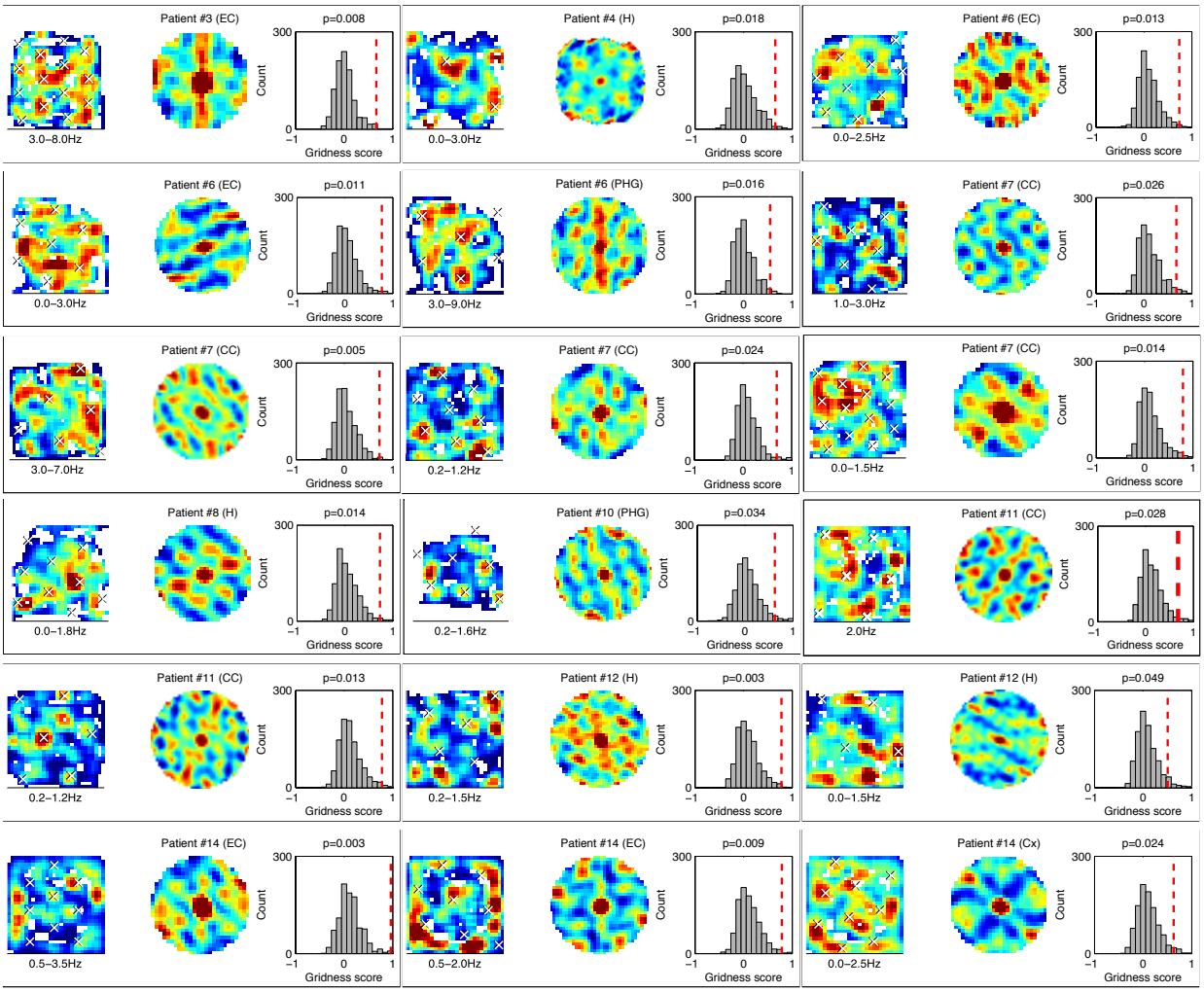

Supplemental Figure S1: **Additional cells that exhibited grid-like spatial firing**. Each panel describes the firing of a neuron that fulfilled our statistical criterion for exhibiting significant grid-like activity. Format for the left and center panels follows Figure 2 in the main manuscript. Text in the upper-right corner indicates the *p* value; label under the left panel indicates the plotted firing-rate range. Right panel illustrates the cell's true gridness score (dashed line) and the distribution of gridness scores from the shuffled data (bars).

Nature Neuroscience: doi:10.1038/nn.3466

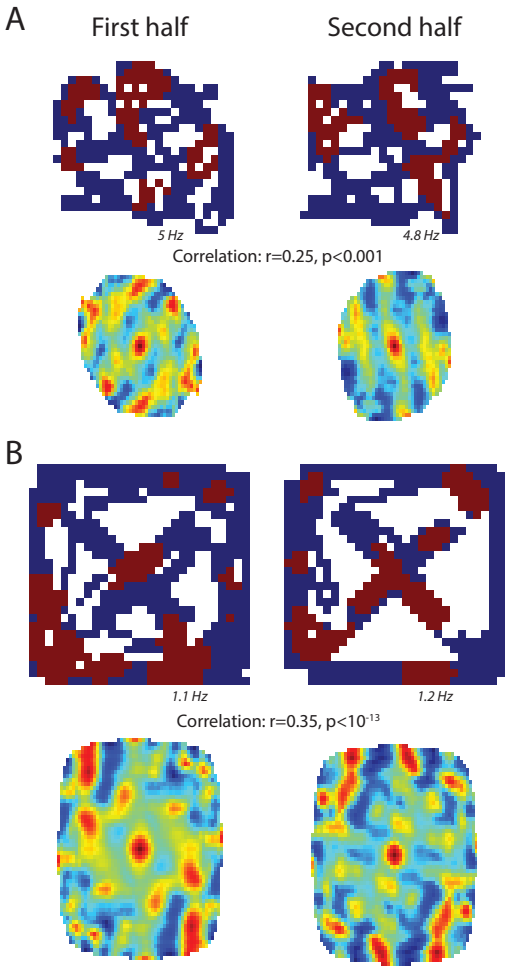

Supplemental Figure S2: **Example grid-like neurons showing significant spatial stability. A.** The activity of a significant grid-like neuron from Patient 10's entorhinal cortex in the first half (left) and the second half (right) of the navigation session. This cell's activity was significantly correlated betwen these two intervals ($p < 0.001$). Top panels depict firing rate maps. Maps are plotted in a thresholded fashion, with red coloring indicating regions with firing above a threshold and blue indicating below-threshold firing (red/blue threshold labeled below plot). Bottom panels depict the cell's spatial autocorrelation functions. **B.** The activity of a significant grid-like neuron from patient 14's entorhinal cortex, which exhibited significantly correlated spatial firing between the two halves of the task ($p < 0.001$). *Population stability analysis of grid-like cells.* We identified grid-like cells using only the first half of each session (to prevent bias) and computed each cell's firing-rate map separately for each half of the session. Then we used a Pearson correlation to compute the pixel-by-pixel similarity between each cell's two maps, assessing statistical significance using a permutation procedure. We observed significant stability at $p < 0.05$ in 12% of the 49 first-half grid-like cells (6 cells) and significant remapping in 0 cells. With a significance threshold of $r > 0.2$, 20% of cells were stable (10) and 1 cell remapped. In both cases, the number of grid-like cells that were stable was reliably more than the number that remapped (p's< 0.02, binomial test).

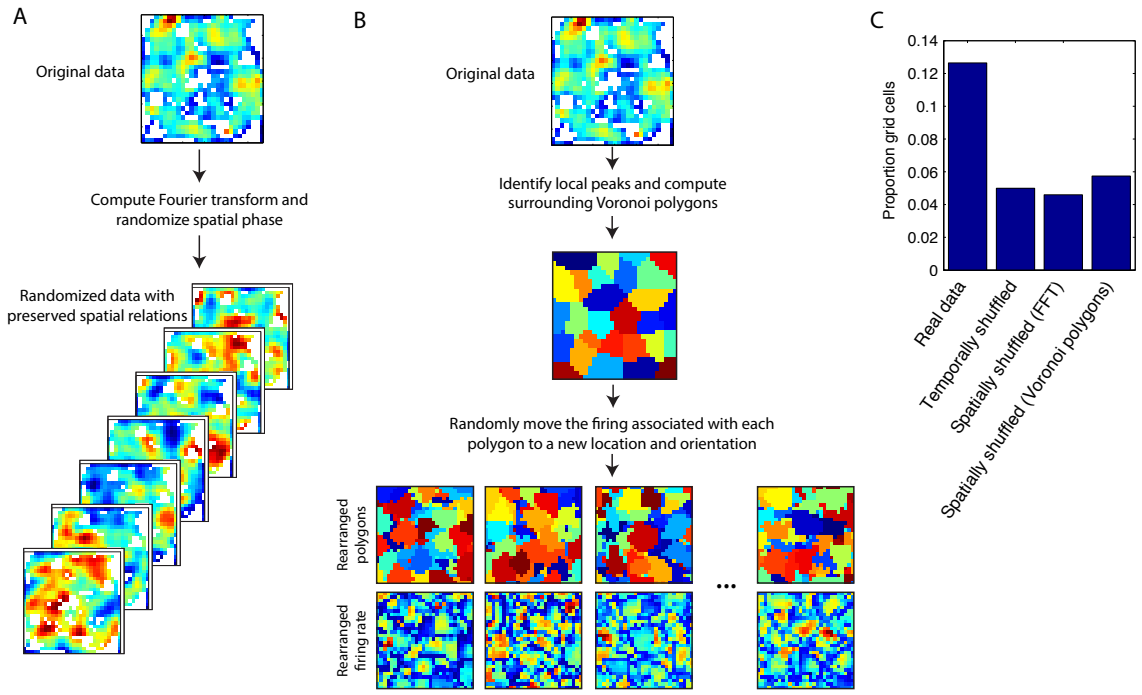

Supplemental Figure S3: **Spatial shuffling control analyses.** These analyses tested whether our findings of significant grid scores could be caused by place cells with multiple place fields that were not specifically arranged in the 60° symmetric pattern of a true grid cell. **A.** Spatial-shuffling procedure based on a Fourier transform. In this procedure we calculated two-dimensional discrete Fourier transform of each cell's firing rate map. Then we generated a series of shuffled surrogate datasets by randomly interchanging the phases of each map's Fourier components and then applying the inverse Fourier transform to calculate a phase-shuffled firing-rate map. This shuffled map has the locations of individual firing fields randomized without significantly changing their size, magnitude, or number. We computed the gridness scores of the shuffled firing maps and measured their significance using the methods from our main analyses. Plots indicate examples of this procedure, with the top panel depicting an example cell's true spatial firing and bottom plots showing example randomized firing maps after shuffling. **B.** Spatial-shuffling procedure based on global shuffling with preservation of local spatial structure. Following the methods of Krupic et al. (2012), we computed each cell's true firing map and then constructed a set of Voronoi polygons surrounding each local firing peak. For each cell we translated and rotated the spiking associated with each polygon to a new random location and orientation in the environment, and then computed the resulting gridness score. This shuffling procedure served as a critical control because it allowed us to verify that the observed gridness scores were truly related to global firing patterns rather than local firing variations, which were preserved within each Voronoi polygon. **C.** Proportion of observed entorhinal cortex grid cells for true and spatially shuffled datasets.

Nature Neuroscience: doi:10.1038/nn.3466

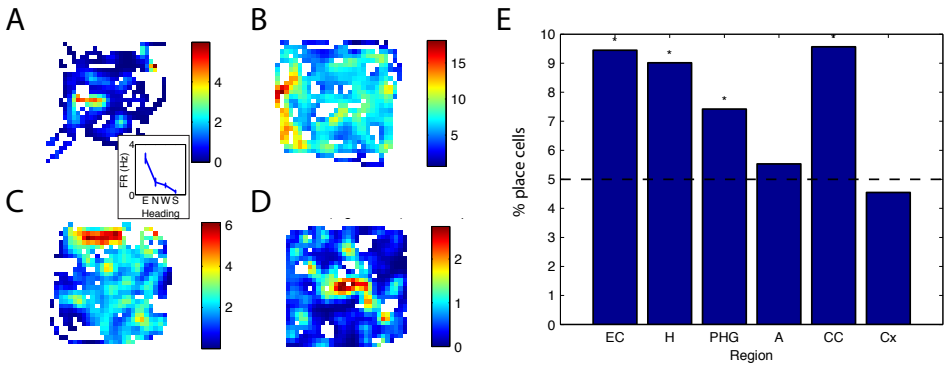

Supplemental Figure S4: **Place cells. A.** A place cell from patient 2's left hippocampus. This cell's activity was significantly elevated during movement in one direction, as detailed in the inset. The color at each location indicates the cell's mean firing rate. **B.** A place cell from patient 5's right hippocampus. **C.** A place cell from patient 9's right parahippocampal gyrus. **D.** A place cell from patient 7's right cingulate cortex. **E.** Prevalence of significant ($p < 0.05$) place cells in each brain region; dashed line denotes the Type 1 error rate. Black asterisks indicate regions where the number of observed cells significantly exceeded chance levels.

Nature Neuroscience: doi:10.1038/nn.3466

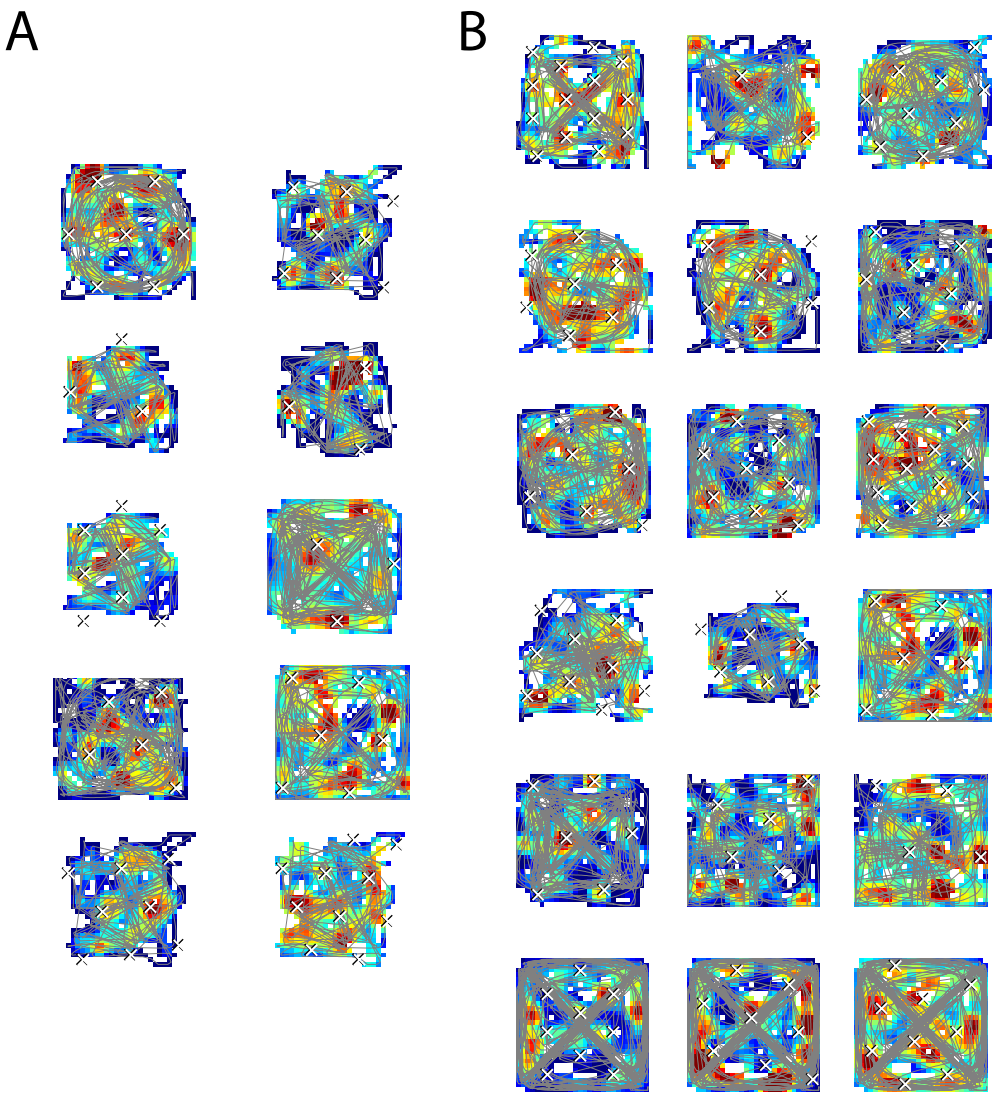

Supplemental Figure S5: **Subject movement in the virtual environment.** Overhead maps of the environment with the subject's movement path plotted as a gray line. Background coloration indicates the cell's firing rate at each location. **A.** The sub-panels of this figure are arranged to match the panels in Figure 2. **B.** The sub-panels of this figure are arranged to match panels from Figure S1.

Nature Neuroscience: doi:10.1038/nn.3466

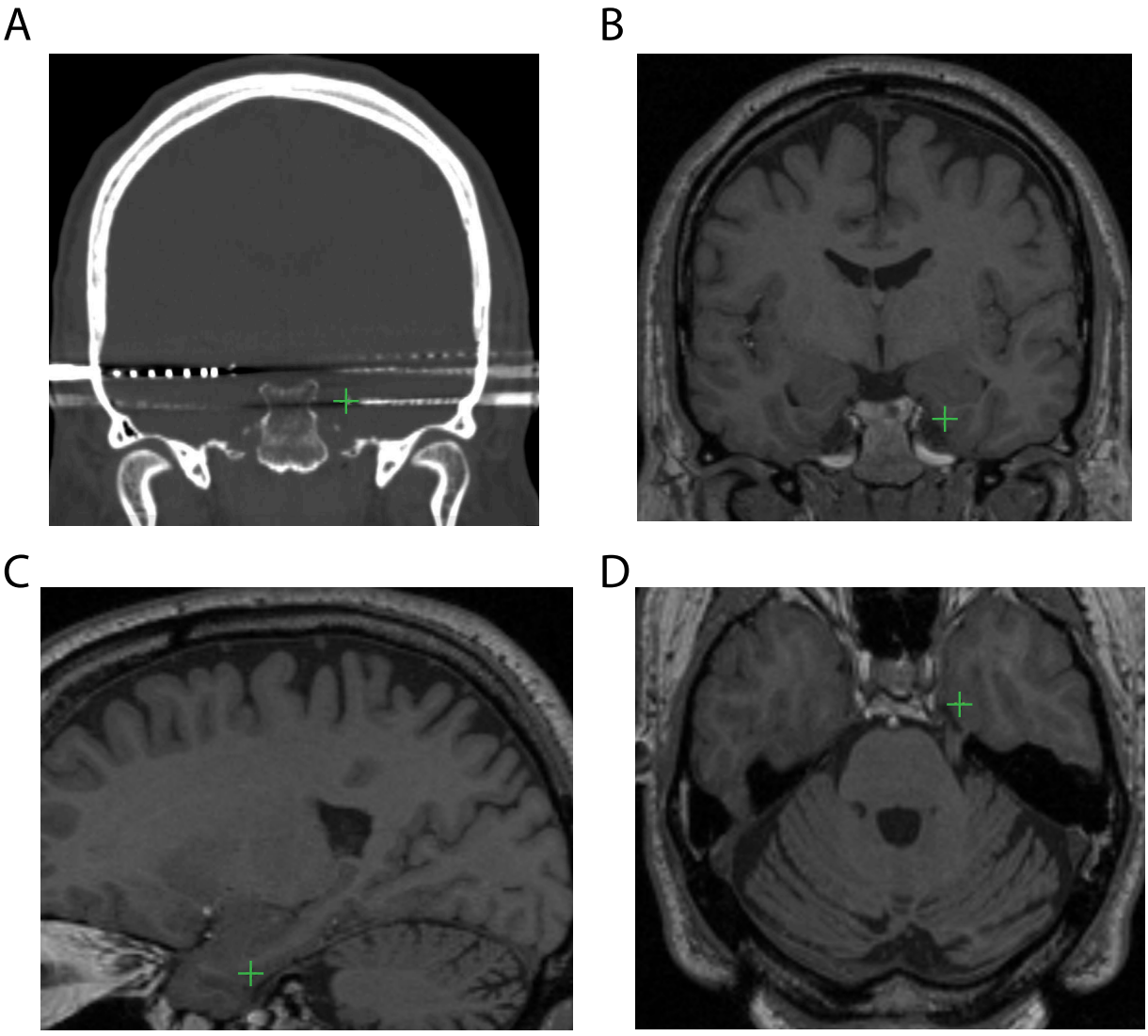

Supplemental Figure S6: **Electrode localization**. Figures depict the localization of a microelectrode bundle in Patient 10's right entorhinal cortex. **A.** Computed tomography (CT) scan after electrode implantation, which shows the electrode positions. The CT image is then co-registered with pre-implantation structural magnetic resonance image (MRI) scans to reveal electrode locations relative to anatomical landmarks. The position of the microelectrode bundle in the left entorhinal cortex is shown by the green crosshairs. **B.** Coronal MRI image. **C.** Sagittal MRI image. **D.** Axial MRI image.

Nature Neuroscience: doi:10.1038/nn.3466

Region	# cells	# grid-like cells	# grid-like cells with direction sensitivity	# grid cells with turn-sensitivity	# grid cells with acceleration sensitivity	# grid with angular-acceleration sensitivity
Entorhinal cortex	89	11	1	4*	2	3
Hippocampus	185	16	5*	1	1	2
Cingulate cortex	156	18	2	2	0	1

Supplemental Table S1: **Grid-like cells that also exhibit direction, turning, acceleration, angular-acceleration-related responses.** Asterisks denote $p < 0.01$, Bonferroni corrected.

	Region						
Subject #	**EC**	**H**	**PHG**	**A**	**CC**	**Cx**	**Unique recording channels**
1	0 of 0	0 of 4	0 of 5	0 of 0	0 of 0	0 of 0	0
2	0 of 0	0 of 12	0 of 0	0 of 0	0 of 0	0 of 0	0
3	1 of 7	0 of 0	1 of 51	0 of 0	0 of 0	0 of 0	2
4	0 of 0	5 of 39	0 of 0	2 of 26	0 of 0	0 of 0	3
5	0 of 0	2 of 34	0 of 0	0 of 0	0 of 0	0 of 0	1
6	3 of 18	0 of 21	1 of 26	0 of 34	0 of 0	0 of 0	3
7	0 of 0	0 of 0	0 of 0	0 of 0	13 of 113	0 of 0	11
8	0 of 0	1 of 8	0 of 22	0 of 19	0 of 0	0 of 5	1
9	0 of 0	1 of 28	2 of 31	2 of 48	0 of 0	0 of 23	4
10	5 of 22	2 of 26	3 of 24	1 of 21	0 of 0	0 of 0	9
11	0 of 11	0 of 0	0 of 2	0 of 0	4 of 30	0 of 5	3
12	1 of 15	3 of 10	0 of 0	0 of 18	1 of 10	1 of 20	6
13	0 of 0	0 of 1	1 of 20	0 of 0	0 of 0	3 of 43	3
14	2 of 16	0 of 2	0 of 0	0 of 4	0 of 3	1 of 16	3
Total	12 of 89	14 of 185	8 of 181	5 of 170	18 of 156	5 of 112	49

Supplemental Table S2: **Summary of grid-like cells across patients.** Table indicates the total number of cells and the number of grid-like cells for each patient, aggregated by brain region. The right-most column indicates the number of grid-like cells observed on unique recording channels across sessions of the task.

Nature Neuroscience: doi:10.1038/nn.3466

Region	Mean Firing Rate (Hz)	Firing Rate 5%–95% range (Hz)	Mean spike amplitude (μV)	Background noise (μV)	Mean false positive (FP) rate	FP below 10%	FP below 20%	Mean false negative (FN) rate	FN below 10%	FN below 20%
Entorhinal cortex	2.8	0.01–9.9	62.4	14.4	9.6%	71%	87%	14%	73%	84%
Hippocampus	3.5	0.03–14.8	51.6	9.6	9.7%	70%	87%	31%	73%	78%
Parahippocampal Gyrus	2.6	0.06–8.9	35	7	11%	65%	75%	17%	77%	80%
Amygdala	1.7	0.09–5.5	50.4	9.4	7.5%	81%	87%	9.1%	88%	91%
Cingulate cortex	3.2	0.1–14.3	43.4	9.3	6.9%	83%	89%	9.9%	85%	87%
Temporal cortex	3	0.1–11.9	65.4	16.4	10%	79%	88%	49%	76%	80%

Supplemental Table S3: **Statistics on cell isolation quality for neurons from each region.** Statistics computed from each neuron's waveform shape using methods described by Hill et al. (2011). False-positive rate indicates the estimated percentage of spikes that were inappropriately designated as belonging to that neuron (instead they came from noise or a neighboring cell). False-negative rate indicates the percentage of spikes that were caused by a given neuron but were inappropriately labeled as members of neighboring clusters or noise. Overall, the vast majority of cells had false-positive and false-negative confusion rates below 10%, consistent with recordings from animals. We compared the spike waveforms of putative grid-like cells with those of other neurons and did not find any differences in their mean amplitude (48 μV for grid cells vs. 46 μV for other cells; $p > 0.95$, t test) or in our false-positive or false-negative rates in distinguishing their waveforms from neighboring cells (p's> 0.5)